A new hyperelastic model for the multi-axial deformation of blood clots occlusion in vessels

Behrooz Fereidoonnezhad[1], Kevin M. Moerman[1], Patrick J. McGarry[1,]*
[1] Biomedical engineering, National university of Ireland Galway, Galway, Ireland

Abstract

Mechanical thrombectomy can be significantly affected by the mechanical properties of the occluding thrombus. In this study we provide the first characterization of the volumetric behaviour of blood clots. We propose a new hyperelastic model for the volumetric and isochoric deformation of clot. We demonstrate that the proposed model provides significant improvements over established models in terms of accurate prediction of nonlinear stress-strain and volumetric behaviours of low and high haematocrit clots. We perform a rigorous investigation of the factors that govern clot occlusion of a tapered vessel. The motivation for such an analysis is two-fold: (i) the role of clot composition on the in-vivo occlusion location is an open clinical question that has significant implications for thrombectomy procedures; (ii) in-vitro measurement of occlusion location in an engineered tapered tube can be used as a quick and simple methodology to assess the mechanical properties/compositions of clots. Simulations demonstrate that both isochoric and volumetric behaviour of clots are key determinants of clot lodgement location, in addition to clot-vessel friction. The proposed formulation is shown to provide accurate predictions of in-vitro measurement of clot occlusion location in a silicone tapered vessel, in addition to accurately predicting the deformed shape of the clot.

Keywords: Acute ischemic stroke, Thrombus, Clot occlusion, Constitutive model, Volumetric behaviour, Thrombectomy

[*] Corresponding author: Patrick.mcgarry@nuigalway.ie

1. Introduction

Acute Ischemic Stroke (AIS), due to embolic occlusion of a cerebral artery, results in over 5.5 million deaths each year. Intra-arterial mechanical thrombectomy (MT) is a minimally invasive procedure in which the obstructing thrombus is removed using a stent-retriever and/or an aspiration catheter. The success of the thrombectomy procedure can be significantly affected by the mechanical properties of the occluding thrombus [4,15]. A thrombus or blood clot is made up of a network of fibrin, platelets, red blood cells (RBCs), and other blood components. Clot mechanical properties are strongly influenced by composition and the arrangement of components within the clot. Previous studies have carried out a variety of mechanical testing on thrombus material, including compression testing [2,4,19,22,33], uniaxial and biaxial tensile testing [4,12,13,23,33], rheometry [5,18,22], nanoindentation [34,35] and friction testing [14]. The extent and composition of the occlusive clot itself influences the therapeutic efficacy of revascularization techniques, yet clot location may be equally important because of the nature and degree of collateral compensation beyond the occlusion [20].

Computational analysis is widely used for pre-clinical assessment of medical devises [1,32,36]. In this context, development of accurate biomechanical material models for blood clots is a key for accurate device simulation and analysis. Incompressibility is commonly assumed in computational modelling of soft tissue, though recent investigations have challenged such assumption [11,24,28]. Blood clots undergo large multi-axial deformations during vessel occlusion, and also during thrombectomy procedures. However, the relative contributions of volumetric and isochoric material behaviour have not previously been investigated.

Therefore, the main motivations/objectives of this study are as follows:

1. Develop and validate a new material model for the volumetric and isochoric mechanical behaviour of blood clots.

2. Investigate the relationship between clot composition/mechanical behaviour and the location at which a clot occlusion occurs in a tapered vessel.

The paper is structured as follows. In Section 2, we calculate the volume change of blood clot analogues during unconfined compression tests for two clot compositions:

a fibrin-rich 5% haematocrit (H) clot; and a RBC-rich 40% H clot. A new volumetric and isochoric hyperelastic model for clots is presented and is shown to accurately reproduce non-linear stress-strain data and non-linear volumetric data for both compositions. In Section 3 we investigate the influence of clot mechanical properties on occlusion location in a tapered vessel. Following a preliminary analysis to clearly parse the sensitivity of the final lodged position of the clot to isochoric and volumetric deformation regimes, we demonstrate that the new constitutive material model accurately replicates clot occlusion locations measured in vitro. Finally, we simulate clot occlusion in a patient-specific artery.

2. Constitutive modelling of blood clots

2.1. Constitutive law for isochoric and volumetric behaviour of blood clots

The hyperelastic BLM model recently proposed by Fereidoonnezhad and McGarry[10] is extended to model the volumetric and isochoric behaviour of blood clots. The isochoric strain energy density function is given as

$$\psi_{iso}(\bar{\lambda}_1, \bar{\lambda}_2, \bar{\lambda}_3) = \sum_{i=1}^{3} \bar{\psi}(\bar{\lambda}_i),$$

$$\bar{\psi}(\bar{\lambda}_i) = \begin{cases} E_1(\bar{\lambda}_i - \ln \bar{\lambda}_i - 1) & |\bar{\lambda}_i - 1| \le D_1 \\ p\left(\frac{\bar{\lambda}_i^{\,2}}{2} - 2\bar{\lambda}_i + \ln \bar{\lambda}_i\right) + q(\bar{\lambda}_i - \ln \bar{\lambda}_i) + r \ln \bar{\lambda}_i + \psi_{01} & D_1 < |\bar{\lambda}_i - 1| < D_2 \\ E_2(\bar{\lambda}_i - (1 + D_2) \ln \bar{\lambda}_i) + (pD_2^2 + qD_2 + r) \ln \bar{\lambda}_i + \psi_{02} & |\bar{\lambda}_i - 1| \ge D_2 \end{cases} \quad (1)$$

where $D_1, D_2, E_1,$ and E_2 are material parameters, $\bar{\lambda}_i$ $(i = 1,2,3)$ are the isochoric principal stretches, $J = \lambda_1\lambda_2\lambda_3$ is the jacobian, and ψ_{01} and ψ_{02} are two constants which ensure the continuity of strain energy. Moreover $p, q,$ and r are not independent parameters; in order to maintain C^0 and C^1 continuity the following relations must be enforced:

$$p = \frac{E_1 - E_2}{2(D_1 - D_2)}, \quad q = E_1 - 2D_1 p, \quad r = (E_1 - q)D_1 - pD_1^2 \quad (2)$$

In the current study we propose an extension of this framework to account for non-linear volumetric behaviour. Building upon to equation (1), a new volumetric strain energy density function is implemented such that:

$$\psi_{vol}(J) = \begin{cases} \kappa_1(\mathrm{J} - \ln \mathrm{J} - 1) & |\mathrm{J} - 1| \leq D_{1v} \\ p_v\left(\frac{\mathrm{J}^2}{2} - 2J + \ln \mathrm{J}\right) + q_v(\mathrm{J} - \ln \mathrm{J}) + r_v \ln \mathrm{J} + \psi_{01v} & D_{1v} < |\mathrm{J} - 1| < D_{2v} \\ \kappa_2(\mathrm{J} - (1 + D_{2v}) \ln \mathrm{J}) + (p_v D_{2v}^2 + q_v D_{2v} + r_v) \ln \mathrm{J} + \psi_{02v} & |\mathrm{J} - 1| \geq D_{2v} \end{cases} \quad (3)$$

in which κ_1 and κ_2 are the initial small-strain and large-strain bulk modulus, respectively, the parameters D_{1v} and D_{2v} control the transition volumetric strains, and $p_v, q_v,$ and r_v are obtained in a similar manner as equation (2) by using the corresponding volumetric parameters. The total strain energy density of the clot material is given as $\psi = \psi_{iso}(\bar{\lambda}_1, \bar{\lambda}_2, \bar{\lambda}_3) + \psi_{vol}(J)$. Stress-strain relationships are readily derived from (1) and (2) above, as described by Fereidoonnezhad and McGarry [10].

2.2. Experimental characterisation of clots and of constitutive law calibration

In Figure 1 we demonstrate that the proposed material formulation accurately reproduces experimentally observed nominal stress-strain behaviour of blood clots subjected to unconfined compression. Specimens are deformed to a nominal compressive axial strain of -0.8 at a compressive strain rate of 0.1 s^{-1} (Figure 1A). Figure 1C shows the experimentally measured stress-strain behaviour for a 40% haematocrit (%H) clot subjected to unconfined compression reported. Corresponding experimental volume changes of the clot during compression are determined using a customised image analysis programme developed in Matlab [24,30]. A highly non-linear relationship between volumetric strain ($\epsilon_v = J - 1$) and compressive axial strain ($\epsilon_a = \lambda_a - 1$) is shown in Figure 1D. Initial axial deformation results in a high rate of volume change (w.r.t applied axial strain, $d\epsilon_v/d\epsilon_a$), suggesting an initially high volumetric. However, a significantly lower rate of volume change is observed for the applied range of axial strain of $0.1 \leq \epsilon_a \leq 0.48$. Finally, the rate of volume change reaches a higher value for $\epsilon_a \geq 0.48$. Full recovery of volumetric strain is observed following retraction of the loading plate. Model predictions of the clot stress-strain behaviour and volume

change are superimposed on Figures 1C-D. The model accurately reproduces the observed complex non-linear experimental behaviour, both in terms of computed nominal stress σ_a (R^2= 0.997) and ε_v (R^2= 0.978), for the entire range of applied axial deformation. Model results suggest that effective tri-linear relationship between ε_v and ε_a, observed experimentally, emerges due to the interaction of material isochoric stiffening and volumetric stiffening. Similar results are presented for fibrin-rich 5% H clots in Figures 1 E-F, again with evidence of bi-linear strain stiffening (Figure 1E). A corresponding increase in the rate of volume change is observed (Figure 1F), such that $d\epsilon_v/d\epsilon_a = 0.0718$ if $\epsilon_a < 0.35$ and $d\epsilon_v/d\epsilon_a = 0.8141$ if $\epsilon_a > 0.55$. However, as shown in Figure 1F, a bi-linear, rather than tri-linear, relationship between ε_v and ε_a is observed experimentally for fibrin-rich 5% H clots ($d\epsilon_v/d\epsilon_a = 0.0718$ for $\epsilon_a < 0.35$ and $d\epsilon_v/d\epsilon_a = 0.8141$ for $\epsilon_a > 0.55$). Again, the computational model accurately reproduces the complex non-linear clot behaviour over the large range of applied axial strain, both in terms of σ_a (R^2= 0.986) and ϵ_v (R^2= 0.957). Best-fit model parameters are listed in Table 1. The experimental and computational investigation of volumetric behaviour of blood clots presented in Figure 1 provides new insight into a key feature of clot behaviour. Previous studies have been limited to the simplified assumption of near incompressible behaviour. The reader is referred to the recent study of Johnson[17] for a full description of the fabrication protocols for clot analogues.

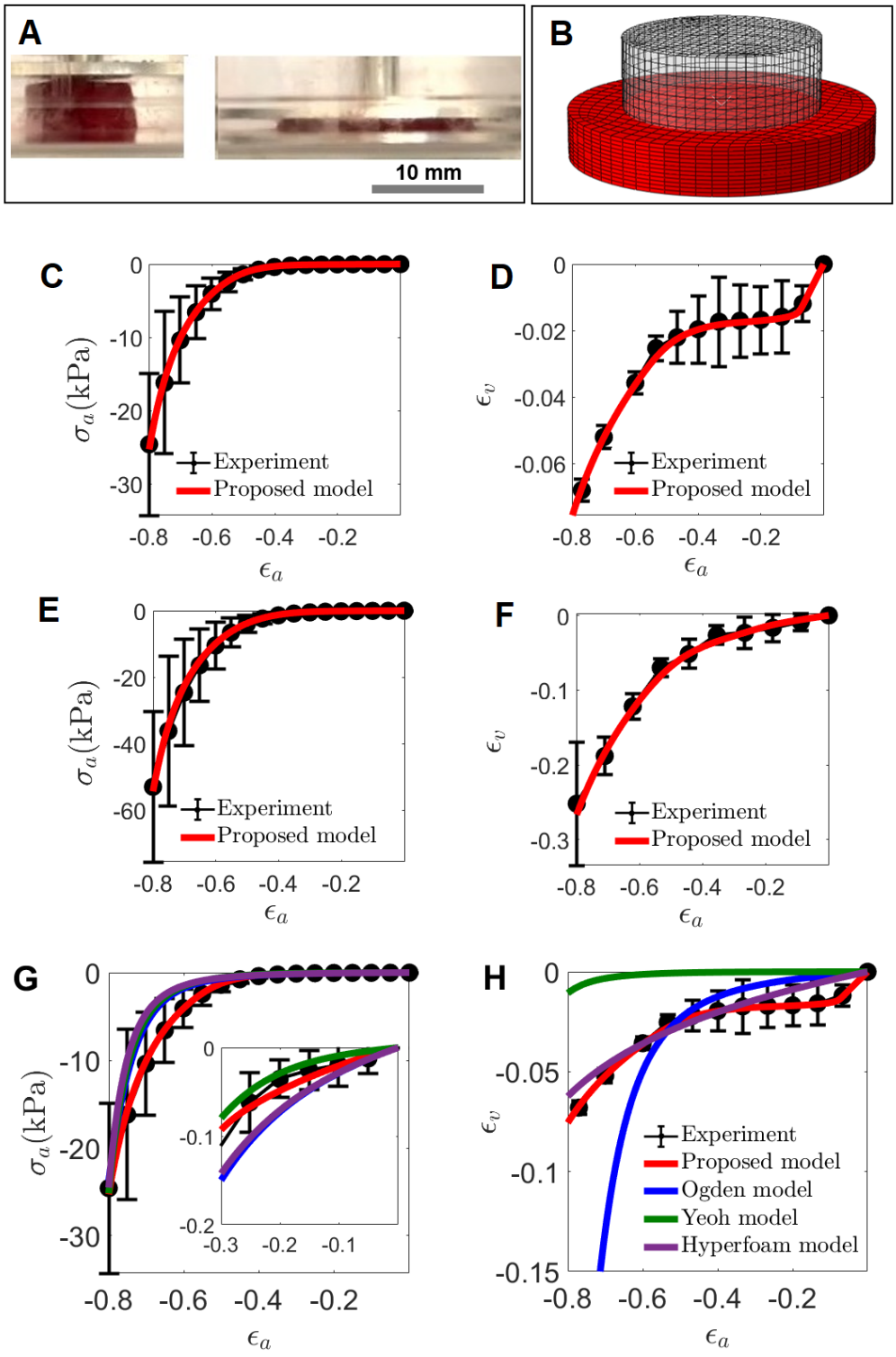

Figure 1: The capability of the proposed model to reproduce the stress-strain experimental data of the unconfined compression of 5% H and 40%H platelet-contracted blood clot analogues [17]. (A) undeformed and deformed blood clot during unconfined compression test; (B) FE simulation of the unconfined compression test; (C, D) Nominal Stress-nominal strain data [17] and volume change for a 40% H platelet-contracted clot; (E, F) Nominal Stress-nominal strain data [17] and volume change for a 5% H platelet-contracted clot. (G, H) Comparing the capability of the proposed model with the well-known hyperelastic laws in reproducing the nominal stress-strain data and the volume change, for the 40% H clot analogue.

Table 1: Material parameters of the proposed model for 5% H and 40% H platelet-contracted clot analogues.

	D_1	D_2	$E_1\,[kPa]$	$E_2\,[kPa]$	D_{1v}	D_{2v}	κ_1	κ_2
5% H	0.13	0.59	0.3	9	0.01	0.05	2	15
40% H	0.25	0.55	0.15	4.1	0.014	0.022	0.5	29

In Figure 1(G,H) we demonstrate that well established and widely implemented hyperelastic formulations are not capable of accurately predicting the non-linear multi-axial behaviour of blood clots shown in Figure 1 above, in contrast to the accurate and robust predictions of our proposed model. Specifically, the Yeoh, Ogden and hyperfoam formulations are investigated. Figure 1(G,H) presents the best-fit prediction for each model, subject to the constraint that all models are calibrated to reproduce experimental value of axial stress at the maximum value of applied axial strain ($\epsilon_a = -0.8$), and the initial axial compressive stiffness ($d\sigma_a/d\epsilon_a\,; -0.1 \leq \epsilon_a \leq 0.0$). Established model formulations and best-fit parameters are presented in Appendix A. In contrast to our proposed formulation, Figure 1G shows that all established models inaccurately predict the tangent stiffness and stress throughout the applied range of ϵ_a. Corresponding predictions of volume change are highly inaccurate for all models for all levels of applied axial strain, as shown in Figure 1H. The inaccuracy of each formulation is quantified in Table 2, in terms of predicted axial stress (σ_a), tangent stiffness, and volumetric strain (ϵ_v) at applied axial strains of 20%, 60%, and 80%. The superior accuracy of the proposed model suggests that blood clots transition from a low constant stiffness regime at low strains to a high constant stiffness regime at high strains, rather than exhibiting continuous power-law or exponential strain stiffening. The accuracy of the non-linear volumetric component of our model suggests that a single parameter (bulk modulus) linear volumetric constitutive law is insufficient for the accurate simulation of large multiaxial large-deformation of clots. In the following sections we demonstrate that both the isochoric and the volumetric behaviour of blood clots are key determinants of the location of clot lodgement in a tapered vessel, thus highlighting the importance of the results presented in Figure 1.

Table 2: Comparing model predictions (proposed (prop.), Ogden, Yeoh, Hyperfoam models) with experimental data for unconfined compression tests of 40% H platelet-contracted clot analogues. The values of nominal axial stress (σ_a), stiffness, and volumetric strain (ϵ_v) at 20%, 60%, and 80% axial compressive strain (ϵ_a) are given. Model errors (%) with respect to experimental data are also indicated.

	$\epsilon_a = 20\%$	$\epsilon_a = 60\%$	$\epsilon_a = 80\%$
	$\sigma_a(kPa)$ [% error]		
Experiment	0.04	4.06	24.58
Prop. model	0.05 [25%]	4.03 [0.8%]	25.28 [2.8%]
Ogden	0.07 [75%]	1.78 [56%]	23.75 [-3.4%]
Yeoh	0.03 [-25%]	1.57 [-62%]	25.17 [2.4%]
Hyperfoam	0.07 [75%]	1.45 [-64%]	24.51 [-0.3%]
	Tangent stiffness (kPa) [% error]		
Experiment	0.37	41.51	171.75
Prop. model	0.33 [-10%]	41.28 [-0.5%]	201.82 [18%]
Ogden	0.56 [53%]	18.90 [-55%]	318.77 [86%]
Yeoh	0.301 [-17%]	17.25 [-58%]	434.45 [153%]
Hyperfoam	0.53 [45%]	14.56 [-65%]	459.65 [168%]
	ϵ_v (%) [% error]		
Experiment	1.68	3.58	6.80
Prop. model	1.70 [1%]	3.62 [1%]	6.80 [0%]
Ogden	0.39 [-77%]	4.97 [39%]	30.51 [350%]
Yeoh	0.005 [-100%]	0.13 [-96%]	0.78 [-89%]
Hyperfoam	0.89 [-47%]	3.60 [1%]	5.81 [-15%]

3. Analysis of the lodgement of blood clots in a tapered vessel

In this section we investigate the influence of clot mechanical properties on the occlusion location in a tapered vessel. The motivation for such an analysis are two-fold: (i) the role of clot composition on the in-vivo occlusion location is a key and open clinical question that could potentially have significant implications for thrombectomy procedures; (ii) in-vitro benchtop measurement of occlusion location in an engineered tapered tube can potentially be used as a quick and simple methodology to assess the mechanical properties/compositions of excised clots or fabricated clot analogues. In the preliminary analysis of Section 3.1 we initially restrict our analysis to quasi-linear material behaviour (i.e. approximately constant stiffness), for both isochoric (shape changing) and volumetric deformation in order to clearly parse the sensitivity of the final lodged position of the clot to both deformation regimes. In Section 3.2 we incorporate non-linear material behaviour, using the calibrated novel constitutive law presented in Section 2 above. We also consider the role of clot rate-dependent visco-hyperelastic on the time-scale required for a clot to reach its final lodged position in Appendix B.

3.1. Linear isochoric and volumetric mechanical behaviour

Figure 2 presents a schematic of the clot and vessel, indicating the key geometric parameters that describe the system and the pressure P_0 applied to the proximal surface of the clot. Several mechanisms govern the final equilibrium position of the clot in the vessel: friction between the clot and the vessel wall, the isochoric deformability of the clot (characterised by the shear modulus $\mu = 3\kappa E/(9\kappa - E)$), and the volumetric compressibility of the clot (characterised by the bulk modulus κ). The equilibrium occlusion location is characterised by the distance u between the centre of the clot at initial contact with the vessel and the and centre of the clot at its final equilibrium position. It should be noted that we present our computed results in non-dimension quantities in order to efficiently demonstrate the key parameter groupings that govern the final equilibrium position of the clot. As a simple example, consider a large and a small clot, both with the same aspect ratio L/D. Of course both clots will initially contact the vessel at different locations, and the larger clot will move a greater

distance u to its final equilibrium position. However, u/D, the non-dimensional measure of the clots' final positions, will obviously be identical in both cases; i.e. for a given clot aspect ratio, u scales with the size of the clot.

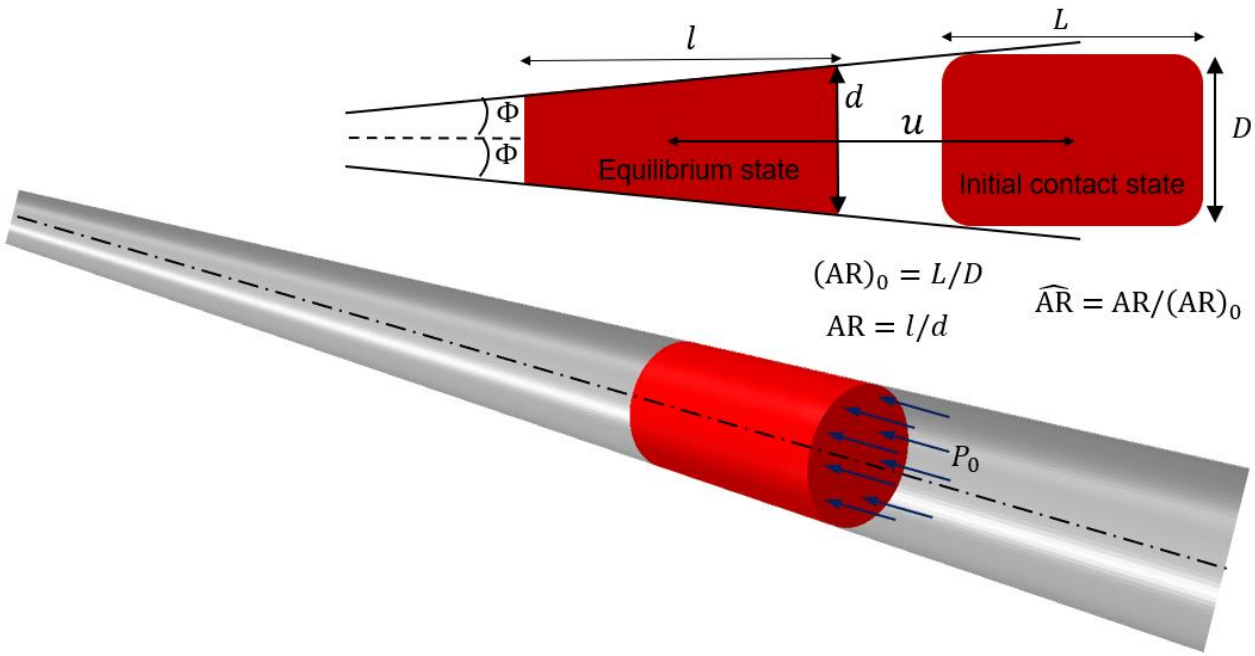

Figure 2: A schematic illustration of the occlusion of a cylindrical blood clot in a tapered vessel. Aspect ratio of clot at initial contact state ($(AR)_0$) and at equilibrium state (AR) as well as the normalized aspect ratio ($\widehat{AR}$) are defined.

Figure 3 shows the results of preliminary parametric study for a vessel with the taper angle of $\Phi = 2^o$. As shown in Figure 3A1, the location of clot lodgement, u, (i.e. the equilibrium position of the clot) for a given applied pressure is strongly dependent on the clot shear modulus for nearly incompressible clots because, in this case, clot cannot change volume and the only deformation mechanism is isochoric shape change, governed by the shear modulus. However, for the case of compressible clots, as shown in Figure 3D1, the final lodged position is not strongly influenced by shear modulus; volume change becomes the dominant mode of deformation. In the physiological cerebral artery blood pressure range (60-100 mmHg [31]) a five-fold increase in shear modulus from 1kPa to 5kPa results in a ~48% decrease in u if a clot is nearly incompressible (Figure 3A1), compared to a ~14% decrease if the clot is compressible (Figure 3D1). It is noted that the range shear modulus (in the small deformation regime) for excised blood clots extends from 18.6 kPa for platelet

contracted/fibrin rich clots down to 0.34 kPa for non-contracted red blood cell rich clots, based on mechanical testing and constitutive modelling of excised clots. The interaction between isochoric and volumetric parameters is further illustrated in Figure 3B1 ($\mu = 5\ kPa$) and Figure 3E1 ($\mu = 50\ kPa$). Beyond a certain level of compressibility ($\kappa \gtrsim 150\ kPa$) the lodged position, u, is insensitive to the value of κ, but strongly dependent on μ (i.e. nearly incompressible clots behave in a similar manner to fully incompressible clots, as demonstrated by the computed value of u for $\kappa = 150\ kPa$ (nearly incompressible) and $\kappa = 2500\ kPa$ (essentially fully incompressible)). However, when the clot is highly compressible, the value of bulk modulus significantly influences the final position; i.e. if kappa is reduced from $150\ kPa$ (nearly incompressible) to $25\ kPa$ (highly compressible), u increases by 45% for low values of shear modulus (Figure 3B) and 62% for high values of shear modulus (Figure 3E1). Figure 3C1, F1 present a preliminary study of the influence of friction coefficient, f, between the clot and the vessel wall for compressible and nearly incompressible clots, respectively. As expected, u increases with decreasing values of f in both cases. However, even for the quasi-linear material behaviour assumed for this preliminary investigation, for any given value of applied pressure P_0, the relationship between f and u is computed to be non-linear. A previous experimental study [14] suggests that the value of f depends on the clot composition; i.e., fibrin-rich blood clots have higher friction coefficient with vessel wall than the RBC-rich clots. Influence of the shear modulus, bulk modules and friction coefficient on the length of the clots are also provided in Figure 3B2-G2.

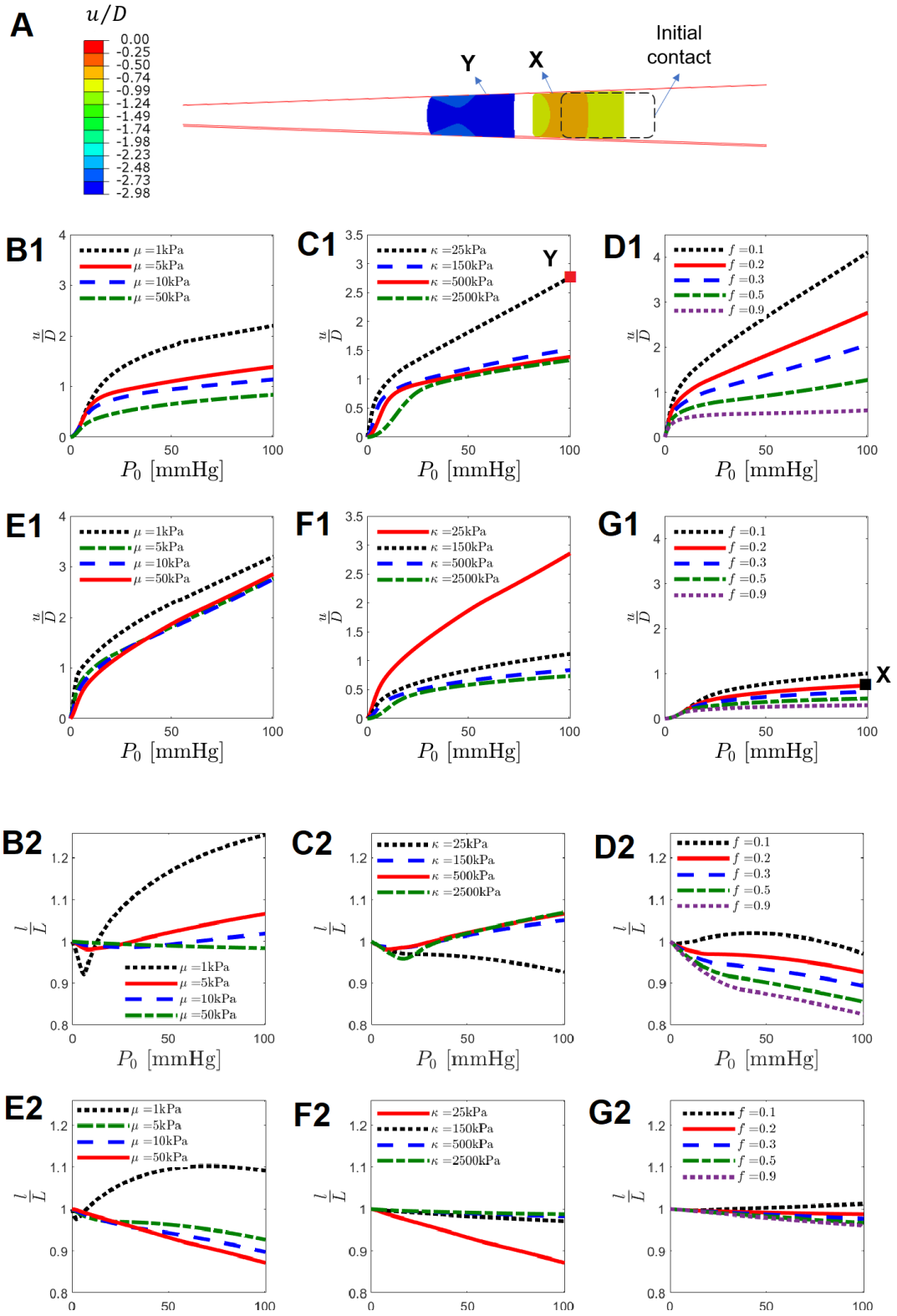

Figure 3: The effects of shear modulus (μ), bulk modulus (κ), and friction coefficient (f) on the occlusion location u in a tapered vessel (B1-G1) and clot length l (B2-G2). The baseline parameters of $L/D = 2, P_0 = 100\ mmHg$, $E_1 = E_2 = 0.0844\ kPa, D_1 = 0.03, D_2 = 0.08, f = 0.2\ and\ \Phi = 2^o$ are used. Also $\kappa = 500\ kPa$, $\kappa = 25\ kPa$ have been used in (B1,B2) and (E1,E2), respectively; $\mu = 5\ kPa, \mu = 50\ kPa$ have been used in (C1,C2) and (F1,F2), respectively; $\mu = 5\ kPa$, $\kappa = 25\ kPa$ have been used in (D1,D2), and $\mu = 50\ kPa$, $\kappa = 2500\ kPa$ have been used for (G1,G2).

In Figure 4 we further explore the preliminary results by considering the computed values of u, l and $\widehat{\mathrm{AR}}$ at a fixed physiological pressure of $P_0 = 100\ \mathrm{mmHg}$. Figure 4A demonstrates the non-linear dependence of u, l and $\widehat{\mathrm{AR}}$ on shear modulus, while Figure 4B demonstrates the high level of sensitivity of u, l and $\widehat{\mathrm{AR}}$ to bulk modulus below a threshold value of compressibility ($\kappa/P_0 \lesssim 4$), and a contrasting insensitivity to bulk modulus above this threshold value. Figure 4C shows the influence of the aspect ratio of the clot ($(AR)_0 = L/D$) on the final equilibrium position, length and final aspect ratio of clot ($\mathrm{AR} = l/d$). As L/D increases (i.e. as a clot of a given diameter becomes longer), the distance travelled (u/D) and the length of clot (l/D) decreases while the aspect ratio (AR) shows a non-monotonic response. This highly non-linear phenomenon is explained in part by the increased friction resistance for longer clots. This model predictions is consistent with the clinical observation that a shorter thrombus is more likely to have a distal location [3,6]. Finally, in Figure 4D we assess the influence of tapered angle of the vessel on u, l and $\widehat{\mathrm{AR}}$. As expected, the value of u is highly sensitive to an increase in taper angle. These analyses can guide the design of tapered-vessel experiments so that the taper angle results in a test system sensitivity range that is capable of differentiating between physiologically relevant clot compositions.

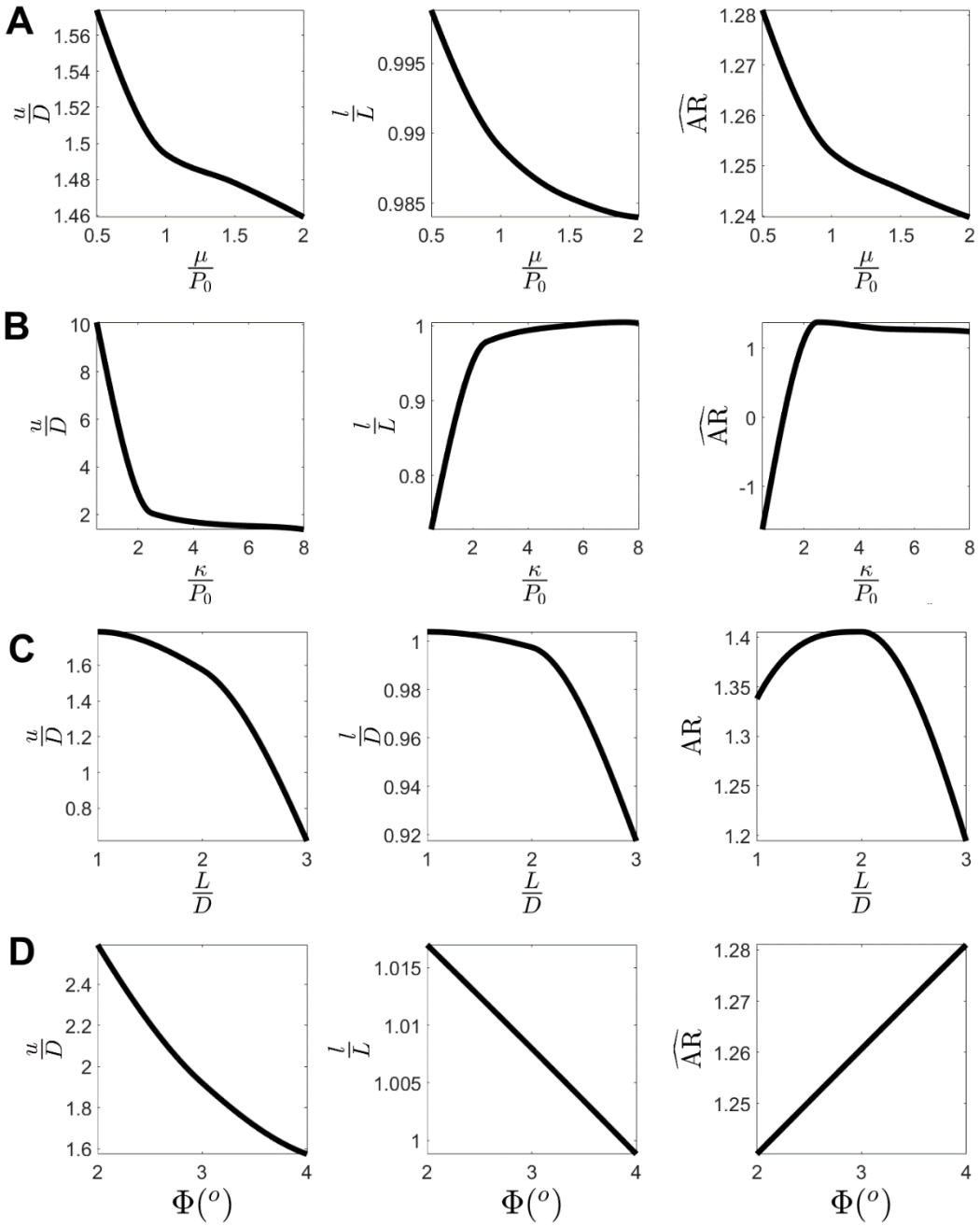

Figure 4: Influence of (A) the shear modulus μ, (B) the compressibility of clot κ, (C) length to diameter ratio of clot L/D, and (D) tube angle (Φ) on the clot travel through the tapered vessel, length of clot and aspect ratio of clot. Baseline parameters of $L/D = 2, P_0 = 75\ mmHg, \mu = 5\ kPa,\ \kappa = 25\ kPa, E_1 = E_2 = 14.06\ kPa,\ D_1 = 0.03, D_2 = 0.08, f = 0.1, and\ \varphi = 4^o$ are used.

The results presented in Figure 3 and Figure 4 take into account the influence of single system parameters on the occlusion location, assuming a base-line reference value for all other system parameters. Such preliminary analyses provide a reasonable introduction to the governing mechanism of clot occlusion in a tapered vessel.

However, in reality all parameters interact with one another, requiring the computation of response surfaces to provide a more detailed understanding of the system. Such response surfaces for paired-interactions between key system parameters are shown in Figure 5. Figure 5A1 presents a 3D surface that elucidates the $\kappa - \mu$ interactions introduced in Figure 4 above. Figure 5B1 demonstrates that u is sensitive to μ for lower value of friction coefficient, f, while it is insensitive to shear modulus for high values of f. Similar sensitivities are observed in the $\kappa - f$ interactions (Figure 5C1). Figure 5D1 shows the interaction of taper angle, Φ, with f. For very high friction values, u is insensitive to Φ, i.e. once the clot initially contacts the tube, it almost immediately becomes lodged, without significant volumetric or isochoric deformation. However, as f reduces, the sensitivity to Φ increases. Similarly, the sensitivity of u to the values of both κ and μ is increased if the value of Φ is reduced. In summary, a tapered-tube experimental system should implement sufficiently low values of Φ and f so that the measured value of u is sensitive to the clot mechanical properties/composition. Figure 5G1 demonstrates interactions between clot aspect ratio (L/D) and f, while Figure 6H1 demonstrates the interaction between L/D and κ. A low level of sensitivity of u to κ is computed for extremely long clots. This is in part, due to a more dominant role of frictional resistance with increasing clot length. Therefore, low aspect-ratio clots should be used experimentally $L/D < 3$ so that the system is sensitive to the clot material properties. The response surfaces for the influence of the parameters on the length of the clots are also provided in Figure 5A2-H2.

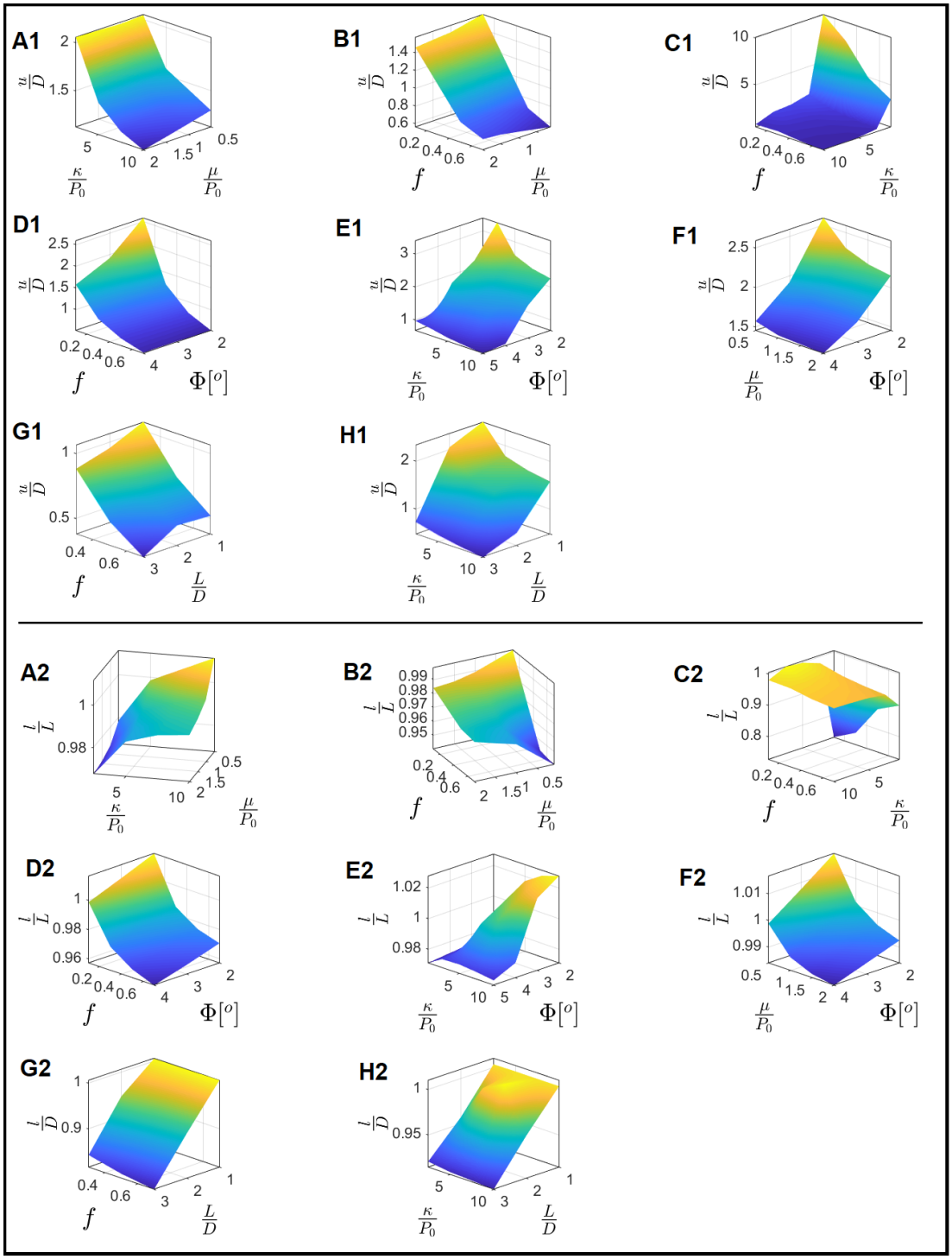

Figure 5: Interactions of the model parameters influencing the occlusion location of blood clot and length of clot in a tapered vessel. The baseline parameters are: $L/D = 2, P_0 = 75\ mmHg, \mu = 5\ kPa,\ \kappa = 25\ kPa, E_1 = E_2 = 14.06\ kPa,\ D_1 = 0.03, D_2 = 0.08, f = 0.1, and\ \Phi = 4^o$.

3.2 Realistic non-linear clot behaviour and vessel deformability

As demonstrated in Figure 1, blood clots exhibit significant volumetric and isochoric strain-stiffening [17]. Here, we use the proposed constitutive model in Section 2 to investigate the influence of clot stiffening on the distance travelled (u/D) in a taper tube. The baseline material parameters are chosen to be the same as those presented in Table 1 for 5% H platelet-contracted clot. Figure 6 demonstrates that for the given parameter sets, strain stiffening of the clot strongly influences the occlusion location. Figure 6B demonstrate that if the stiffening ratio ($\mathrm{E}_2/\mathrm{E}_1$) is increased from 1 to 10, u decreases by 18%. The results of Figure 6D shows even an stronger influence of volumetric stiffening (κ_2/κ_1) on u. Increasing κ_2/κ_1 from 1 to 10 results in a 38% decrease in the value of u. Such sensitivity to κ_2/κ_1 is less pronounced beyond the threshold of $\kappa_2/\kappa_1 > 20$. Figure 6A, C show that u increases with increasing values of the transition strains D_1 and D_{1v}. Increasing the transition strains postpones the start of clot stiffening, allowing the clot to travel further into the tapered tube.

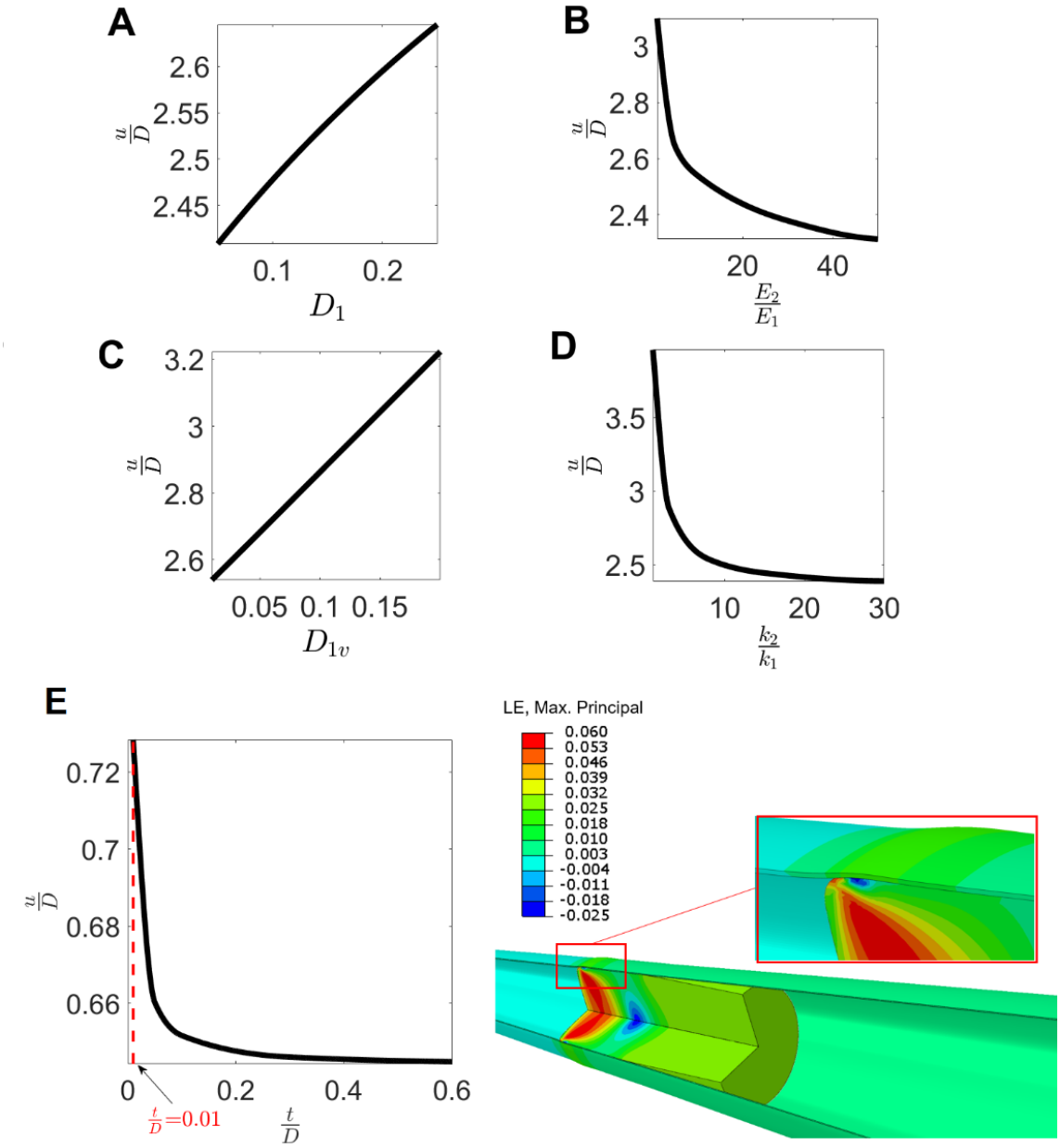

Figure 6: Influences of clot strain-stiffening on occlusion location. Effect of (A) the transition strain, D_1; (B) stiffening ratio E_2/E_1; (C) volumetric transition strain D_{1v}, and (D) bulk modulus ratio κ_2/κ_1 are illustrated. The baseline material parameters are taken from Table 1 for 5% H platelet-contracted clot and $L/D = 2$, $P_0 = 75\ mmHg$, $f = 0.2\ and\ \Phi = 2^o$ are used. The value of $D_2 - D_1$ and $D_{2v} - D_{1v}$ are kept constant. Influences of tube thickness on the occlusion location for a silicone tapered tube and the deformed shape of the clot in a thin tube (t/D=0.01) is also shown in (E). The inset shows bulge in the tube.

The validity of modelling the tapered vessel as a rigid body is investigated by incorporating the effect of tube compliance and thickness in the FE simulations. Silicon rubber tubes with a range of thicknesses are considered and the variation of occlusion

location with tube thickness is shown in Figure 6E. Results are sensitive to the wall thickness of a silicone tube only if the tube wall thickness is less than 5% of the clot diameter. As an example, for a clot of 5mm diameter, the tube can reliably be modelled as a rigid material provided that the tube wall thickness is greater than ~250 μm. In Section 3.3 the non-linear compliance of a cerebral artery is taken into account in the simulation of clot occlusion in a patient-specific vessel anatomy.

3.3. Simulation of in-vitro tapered vessel experiment and in-vivo patient specific clot occlusion

In addition to the detailed analysis presented above, we have also implemented In a parallel experimental study we performed a series of experiments in which clot analogues were introduce into a tapered vessel and the final occlusion location is measured. In summary, a silicone tube with taper angle $\Phi = 0.9854^{o}$ was fabricated, with cylindrical clot analogue specimen of length of 15 mm and diameter of 5.3 mm. Applied pressures of 90 mmHg and 30 mmHg were applied to the proximal and distal surface of the cylindrical clots, respectively. The reader is referred to the parallel study [16] for details of experiment set-up and clot fabrication, in addition to a detailed presentation of experimental measurements for a wide range of clot compositions. Here we provide preliminary simulations of the occlusion of a 5%H and a 40%H to demonstrate the volumetric and isochoric hyperelastic formulations introduced in the current study provide accurate predictions of experimentally measured clot occlusion locations and deformation. The friction coefficients of $f = 0.09$ and $f = 0.05$ have been used for the contact between the silicone surface and 5%H and 40%H clot analogues, respectively. It is noted that there is no published data for the friction coefficient between a silicone surface and blood clot. However, based on the previous measurement of the static friction coefficient between PTFE and clot analogues [14] the friction coefficient for a fibrin-rich clot is ~1.8 times higher than the friction coefficient for a RBC-rich clot.

The results, as demonstrated in Figure 7, show a reasonable agreement between computational results and the in-vitro data in terms of the distance that clot travel into the tube (u/D) and the deformation of the clot, characterised by the deformed aspect ratio ($\widehat{\mathrm{AR}}$). We highlight that the isochoric and volumetric behaviour of clot as well as

the friction coefficient contribute in these two measurable quantities. Despite the fact that the 5% H clot has a higher isochoric tangent modulus and friction coefficient, it travels farther into the tapered vessel than the 40% H clot. This is due to the higher level of compressibility (volumetric deformability) of the 5% H clot. This suggests that non-linear hyperelastic volumetric behaviour is a key determinant of the occlusion location of a clot. This further highlights the importance of the accurate characterization of and constitutive modelling of the volumetric behaviour of a range of clot compositions.

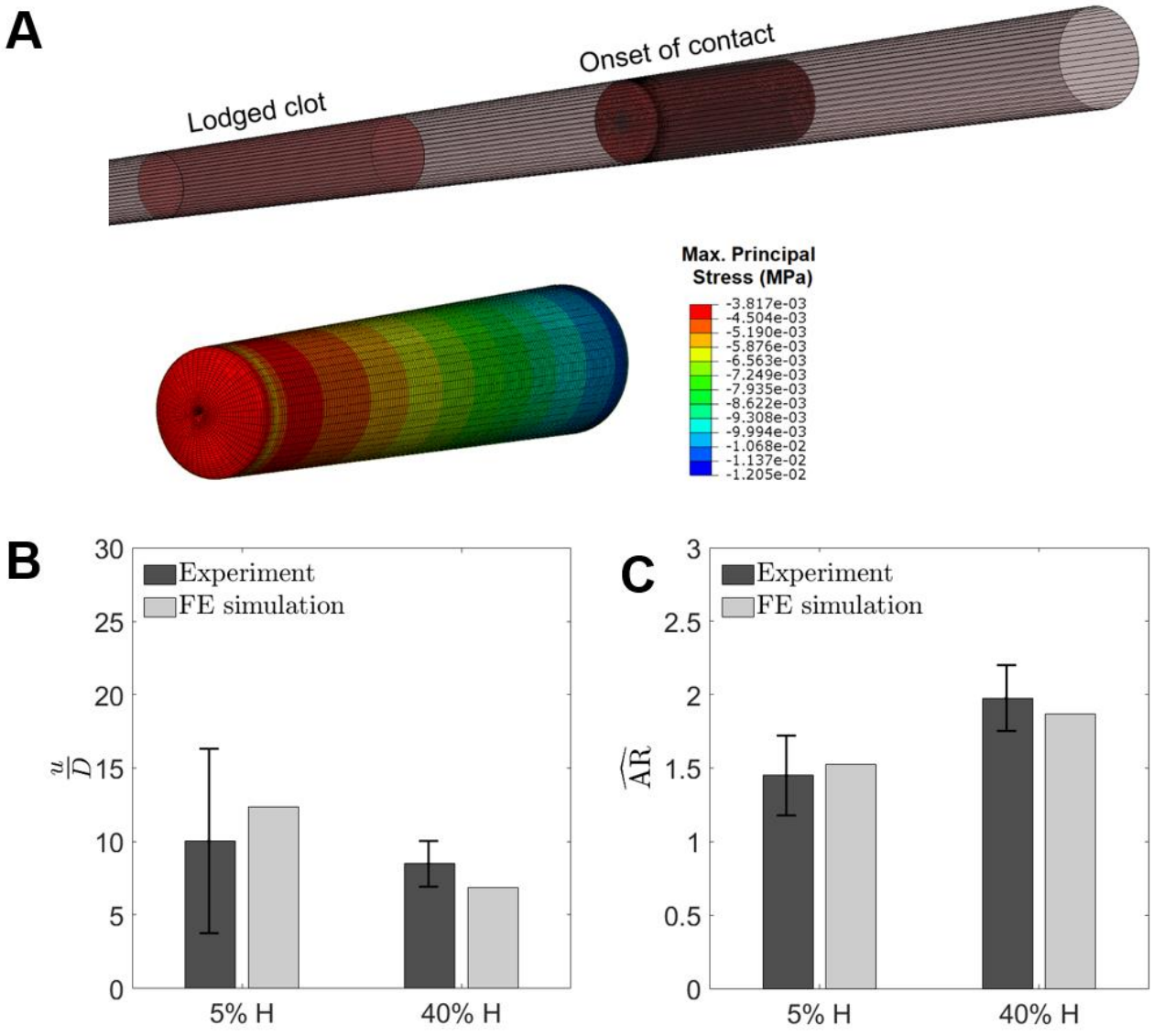

Figure 7: Comparison of in-vitro and FE results for occlusion of the platelet-contracted blood clot analogues in a silicon rubber vessel with taper angle of $\Phi = 0.9854^{o}$. (A) FE simulation results for the 40% H platelet-contracted clot analogues. (B) The location of clot lodgement (u/D) and (C) aspect ratio of clot ($\widehat{AR}$) for 5% H and 40% H clot. The material parameters from Table 1 have been employed.

Finally, we simulate clot occlusion in a patient-specific cerebral artery A 40% H platelet-contracted clot is inserted into The vessel geometry is reconstructed from clinical CT images using the GIBBON toolbox [27]. The mechanical behaviour of the vessel is based on the experimental test data for cerebral arteries reported by Monson et al.[29].. Friction coefficient of 0.3 has been used for the contact between artery and clot. A 40% H clot is introduced into the vessel (FigureA) with a pressure $\mathrm{P}_0 = 75\ \mathrm{mmHg}$ applied to the proximal face of the clot to approximate in-vivo physiological loading.

FigureA (top) illustrates the clot at initial point of contact between the clot and the vessel. The final computed deformed clot at the location of occlusion is also shown in FigureA (bottom row – three views shown to illustrate vessel tortuosity). The computed distribution of maximum shear stress in the clot at lodged position is shown in FigureB. This simulation highlights the significant deformation and stress in the clot at its occluded location. Such predicted stress distributions could be included in FE simulations of clinical interventions, such as thrombectomy and aspiration [21] to provide improved predictions of the interaction between the clot and the intervention device and may also provide improved prediction of clot fragmentation risk during thrombectomy procedures. Finally, the strain and deformation of the arterial wall due to interaction with the clot is shown in FigureC. The small values of strain and deformation suggest that modelling the artery geometry as a rigid body is acceptable.

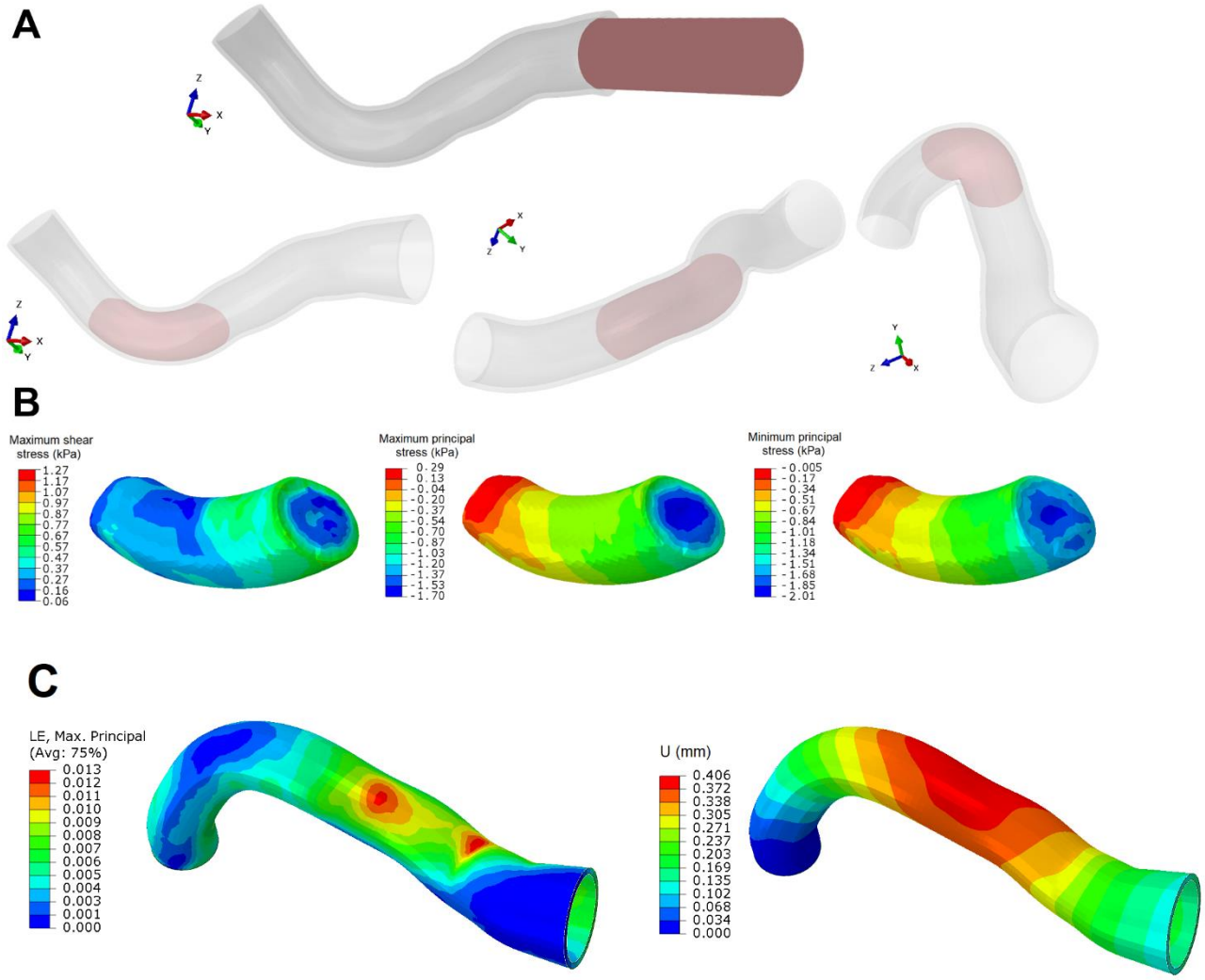

Figure 8: FE prediction of the clot occlusion in a patient-specific cerebral artery for a 40% H platelet-contracted clot analogue. (A) Clot at onset of contact and at lodged position, (B) Cauchy stress distribution in the clot at lodged position, and (C) Maximum principal logarithmic strain and displacement of the vessel wall.

4. Summary and conclusions

Mechanical thrombectomy has become the standard acute ischemic stroke treatment in patients with large vessel occlusion. The success of the thrombectomy procedure can be significantly affected by the mechanical properties of the occluding thrombus. In this study we provide the first characterization of the volumetric behaviour of blood clots. We propose a new hyperelastic model for the volumetric and isochoric deformation of blood clot. We demonstrate that the proposed model provides significant improvements over established hyperelastic models in terms of accurate prediction of nonlinear stress-strain behaviour and non-linear volumetric behaviour of low and high haematocrit blood clots. We perform a rigorous parametric investigation

of the factors that govern clot occlusion of a tapered vessel. The motivation for such an analysis are two-fold: (i) the role of clot composition on the in-vivo occlusion location is a key and open clinical question that has significant implications for thrombectomy procedures; (ii) in-vitro benchtop measurement of occlusion location in an engineered tapered tube can potentially be used as a quick and simple methodology to assess the mechanical properties/compositions of excised clots or fabricated clot analogues. Simulations demonstrate that both the isochoric and the volumetric behaviour of blood clots are key determinants of the location of clot lodgement in a tapered vessel, in addition to clot-vessel friction. The proposed volumetric/isochoric clot hyperelastic formulation is shown to provide accurate predictions of in-vitro measurement so of clot occlusion location in a silicone tapered vessel, in addition to accurately predicting the deformed shape of the clot. These findings provides a significant advance in the current understanding of the relationship between clot mechanical behaviour and occlusion location in cerebral vascular network which can help to guide clinical intervention strategies and development of the next-generation thrombectomy devices

The following key points should be noted:

1. The non-linear volumetric and isochoric hyperelastic constitutive law proposed in this study provide accurate predictions of the complex patterns of experimentally measured stress and corresponding volume change for both RBC-rich clots (40% H) and fibrin-rich clots (5% H). We demonstrate that established hyperelastic models cannot provide comparable levels of accuracy. Therefore, our model predictions suggests that (i) blood clots transition from a low constant stiffness regime at low strains to a high constant stiffness regime at high strains, rather than exhibiting continuous power-law or exponential strain stiffening; (ii) blood clots exhibit a volumetric strain stiffening, and traditionally implemented single parameter (bulk modulus) linear volumetric constitutive laws [8,9,30,32] are not suitable for the simulation of large multiaxial large-deformation of clots. This study provides the first detailed characterisation of the volumetric change for a range of clot analogue compositions.

2. Accurate modelling of volumetric and isochoric behaviour of clots is critical in order to accurately predict clot occlusion location in a tapered vessel. The volumetric and isochoric formulation proposed in the current study is shown to provide a reasonably accurate prediction of in vitro experiments of clot occlusion in a tapered silicone vessel,

both in terms of occlusion location and deformed shape of the clot. Accurate predictions are achieved for both 10% H and 5% H clots compositions. Our simulation of clot occlusion in patient-specific vessel provides a quantitative distribution of stress throughout the clot when lodged in the vessel. This can be used as an initial condition for in silico thrombectomy simulations [21] .

The new understanding of volumetric behaviour of clots will be incorporated into ongoing development of in silico models for thrombectomy procedures. Future simulations will consider the multiaxial deformation of the lodged clot due to deployment of stent retrievers [21]. The rupture risk during thrombectomy and aspiration will be simulated using cohesive zone [25,26] and extended finite element techniques [7] based on an ongoing experimental investigation of the influence of clot composition on fracture resistance.

Acknowledgements

The authors would like to acknowledge Dr. Ray McCarthy and Dr. Sarah Johnson for providing the videos of the unconfined compression tests which were used for volume change calculations. This work was funded by a European Union Horizon 2020 Research and Innovation Program, under grant agreement No. 777072.

References

1. Ajjan, R. A., K. F. Standeven, M. Khanbhai, F. Phoenix, K. C. Gersh, J. W. Weisel, M. T. Kearney, R. A. S. Ariens, and P. J. Grant. Effects of aspirin on clot structure and fibrinolysis using a novel in vitro cellular system. *Arterioscler. Thromb. Vasc. Biol.* 29:712–717, 2009.

2. Ashton, J. H., J. P. Vande Geest, B. R. Simon, and D. G. Haskett. Compressive mechanical properties of the intraluminal thrombus in abdominal aortic aneurysms and fibrin-based thrombus mimics. *J. Biomech.* 42:197–201, 2009.

3. Boodt, N., K. C. J. Compagne, B. G. Dutra, N. Samuels, M. L. Tolhuisen, H. C. B. R. Alves, M. Kappelhof, G. J. Lycklama À Nijeholt, H. A. Marquering, C. B. L. M. Majoie, H. F. Lingsma, D. W. J. Dippel, and A. Van Der Lugt. Stroke Etiology and Thrombus Computed Tomography Characteristics in Patients with Acute

Ischemic Stroke: A MR CLEAN Registry Substudy. *Stroke* 51:1727–1735, 2020.

4. Chueh, J. Y., A. K. Wakhloo, G. H. Hendricks, C. F. Silva, J. P. Weaver, and M. J. Gounis. Mechanical characterization of thromboemboli in acute ischemic stroke and laboratory embolus analogs. *Am. J. Neuroradiol.* 32:1237–1244, 2011.

5. van Dam, Evelyne A. Dams, Susanne D. Peters, Gerrit W.M. Rutten, Marcel C.M.; Schurink, Geert Willem H. Buth, Jaap van de Vosse, F. N. Determination of linear viscoelastic behavior of abdominal aortic aneurysm thrombus - IOS Press. , 2006.at <https://content.iospress.com/articles/biorheology/bir439>

6. Dutra, B. G., M. L. Tolhuisen, H. C. B. R. Alves, K. M. Treurniet, M. Kappelhof, A. J. Yoo, I. G. H. Jansen, D. W. J. Dippel, W. H. Van Zwam, R. J. Van Oostenbrugge, A. J. Da Rocha, H. F. Lingsma, A. Van Der Lugt, Y. B. W. E. M. Roos, H. A. Marquering, and C. B. L. M. Majoie. Thrombus Imaging Characteristics and Outcomes in Acute Ischemic Stroke Patients Undergoing Endovascular Treatment. *Stroke* 50:2057–2064, 2019.

7. Feerick, E. M., X. C. Liu, and P. McGarry. Anisotropic mode-dependent damage of cortical bone using the extended finite element method (XFEM). *J. Mech. Behav. Biomed. Mater.* 20:77–89, 2013.

8. Fereidoonnezhad, B., R. Naghdabadi, and G. A. Holzapfel. Stress softening and permanent deformation in human aortas: Continuum and computational modeling with application to arterial clamping. *J. Mech. Behav. Biomed. Mater.* 61:, 2016.

9. Fereidoonnezhad, B., R. Naghdabadi, S. Sohrabpour, and G. A. Holzapfel. A Mechanobiological model for damage-induced growth in arterial tissue with application to in-stent restenosis. *J. Mech. Phys. Solids* 101:, 2017.

10. Fereidoonnezhad, B., C. O'Connor, and P. McGarry. A new anisotropic soft tissue model for elimination of unphysical auxetic behaviour. *J. Biomech.* , 2020.

11. Gabbay, J. S., P. A. Zuk, A. Tahernia, M. Askari, C. M. O'Hara, T. Karthikeyan, K. Azari, J. O. Hollinger, and J. P. Bradley. *In Vitro* Microdistraction of

Preosteoblasts: Distraction Promotes Proliferation and Oscillation Promotes Differentiation. *Tissue Eng.* 12:3055–3065, 2006.

12. Gasser, T. C., G. Görgülü, M. Folkesson, and J. Swedenborg. Failure properties of intraluminal thrombus in abdominal aortic aneurysm under static and pulsating mechanical loads. *J. Vasc. Surg.* 48:179–188, 2008.

13. Vande Geest, J. P., M. S. Sacks, and D. A. Vorp. A planar biaxial constitutive relation for the luminal layer of intra-luminal thrombus in abdominal aortic aneurysms. *J. Biomech.* 39:2347–2354, 2006.

14. Gunning, G. M., K. McArdle, M. Mirza, S. Duffy, M. Gilvarry, and P. A. Brouwer. Clot friction variation with fibrin content; implications for resistance to thrombectomy. *J. Neurointerv. Surg.* 10:34–38, 2018.

15. Johnson, S., J. Chueh, M. J. Gounis, R. McCarthy, J. P. McGarry, P. E. McHugh, and M. Gilvarry. Mechanical behavior of in vitro blood clots and the implications for acute ischemic stroke treatment. *J. Neurointerv. Surg.* , 2019.doi:10.1136/neurintsurg-2019-015489

16. Johnson, S., B. Fahy, P. McGarry, R. McCarthy, P. E. McHugh, and A. Consoli. Investigating Clot Behaviour and Occlusion Dynamics over the Relevant Timeline for Acute Ischemic Stroke. , Under review, 2020.

17. Johnson, S., Ray McCarthy, Peter McHugh, and P. Mcgarry. Investigating the Mechanical Behaviour of Clot Analogues through Experimental and Computational Analysis. *Ann. Biomed. Eng.* , Accepted-In press, 2020.

18. Kim, J., and M. A. Srinivasan. Characterization of viscoelastic soft tissue properties from in vivo animal experiments and inverse FE parameter estimation. , 2005.

19. Krasokha, N., W. Theisen, S. Reese, P. Mordasini, C. Brekenfeld, J. Gralla, J. Slotboom, G. Schrott, and H. Monstadt. Mechanical properties of blood clots - a new test method. Mechanische Eigenschaften von Thromben - Neue Untersuchungsmethoden. *Materwiss. Werksttech.* 41:1019–1024, 2010.

20. Liebeskind, D. S. Collaterals in acute stroke: Beyond the clot. *Neuroimaging Clin. N. Am.* 15:553–573, 2005.

21. Luraghi, G., J. F. R. Matas, G. Dubini, F. Berti, S. Bridio, S. Duffy, A. Dwivedi, R. McCarthy, B. Fereidoonnezhad, P. McGarry, C. B. L. M. Majoie, and F. Migliavacca. Applicability assessment of a stent-retriever thrombectomy finite-element model. *R. Soc. Interface Focus* , Accepted-In press 2020.

22. Malone, F., E. McCarthy, P. Delassus, P. Fahy, J. Kennedy, A. J. Fagan, and L. Morris. The Mechanical Characterisation of Bovine Embolus Analogues Under Various Loading Conditions. *Cardiovasc. Eng. Technol.* 9:489–502, 2018.

23. Di Martino, E., S. Mantero, F. Inzoli, G. Melissano, D. Astore, R. Chiesa, and R. Fumero. Biomechanics of abdominal aortic aneurysm in the! presence of endoluminal thrombus: Experimental characterisation and structural static computational analysis. *Eur. J. Vasc. Endovasc. Surg.* 15:290–299, 1998.

24. McEvoy, E., G. A. Holzapfel, and P. McGarry. Compressibility and Anisotropy of the Ventricular Myocardium: Experimental Analysis and Microstructural Modeling. *J. Biomech. Eng.* 140:081004, 2018.

25. McGarry, J. P., and P. E. McHugh. Modelling of in vitro chondrocyte detachment. *J. Mech. Phys. Solids* 56:1554–1565, 2008.

26. McGarry, J. P., É. Ó Máirtín, G. Parry, and G. E. Beltz. Potential-based and non-potential-based cohesive zone formulations under mixed-mode separation and over-closure. Part I: Theoretical analysis. *J. Mech. Phys. Solids* 63:336–362, 2014.

27. Moerman, K. M. GIBBON: The Geometry and Image-Based Bioengineering add-On Software • Review • Repository • Archive. , 2018.doi:10.21105/joss.00506

28. Moerman, K. M., B. Fereidoonnezhad, and J. P. McGarry. Novel hyperelastic models for large volumetric deformations. *Int. J. Solids Struct.* 193–194:474–491, 2020.

29. Monson, K. L., W. Goldsmith, N. M. Barbaro, and G. T. Manley. Axial mechanical properties of fresh human cerebral blood vessels. *J. Biomech. Eng.* 125:288–294, 2003.

30. Nolan, D. R., and J. P. McGarry. On the Compressibility of Arterial Tissue. *Ann. Biomed. Eng.* 44:993–1007, 2016.

31. Pires, P. W., C. M. Dams Ramos, N. Matin, and A. M. Dorrance. The effects of hypertension on the cerebral circulation. , 2013.

32. Rouhani, F., B. Fereidoonnezhad, M. R. Zakerzadeh, and M. Baghani. A computational study on vascular damage caused by shape memory alloy self-expandable and balloon-expandable stents in a stenosed artery. *J. Intell. Mater. Syst. Struct.* 30:3113–3123, 2019.

33. Saldívar, E., J. N. Orje, and Z. M. Ruggeri. Tensile destruction test as an estimation of partial proteolysis in fibrin clots. *Am. J. Hematol.* 71:119–127, 2002.

34. Slaboch, C. L., M. S. Alber, E. D. Rosen, and T. C. Ovaert. Mechano-rheological properties of the murine thrombus determined via nanoindentation and finite element modeling. *J. Mech. Behav. Biomed. Mater.* 10:75–86, 2012.

35. Weafer, F. M., S. Duffy, I. Machado, G. Gunning, P. Mordasini, E. Roche, P. E. McHugh, and M. Gilvarry. Characterization of strut indentation during mechanical thrombectomy in acute ischemic stroke clot analogs. *J. Neurointerv. Surg.* 11:891–897, 2019.

36. Zhao, S., L. Gu, and S. R. Froemming. Assessment of shape memory alloy stent deployment in a stenosed artery. *Biomed. Eng. Lett.* 1:226–231, 2011.

Appendix A: Constitutive models formulations and parameters

The model formulations and best-fit parameters for the hyperelastic models used in Section 2 are presented here. The strain energy density function for Ogden model is given as

$$\psi = \sum_{i=1}^{N} \frac{2\mu_i}{\alpha_i^2}\left(\bar{\lambda}_1^{\alpha_i} + \bar{\lambda}_2^{\alpha_i} + \bar{\lambda}_3^{\alpha_i} - 3\right) + \sum_{i=1}^{N} \frac{1}{D_i}(\mathrm{J}-1)^{2i} \tag{A1}$$

where, $\mu_i, \alpha_i,$ and D_i are material parameters. The Yeoh strain energy density function is given as

$$\begin{aligned}\psi = {} & C_{10}(\bar{I}_1 - 3) + C_{20}(\bar{I}_1 - 3)^2 + C_{30}(\bar{I}_1 - 3)^3 \\ & + \frac{1}{D_1}(\mathrm{J}-1)^2 + \frac{1}{D_2}(\mathrm{J}-1)^4 + \frac{1}{D_3}(\mathrm{J}-1)^6,\end{aligned} \tag{A2}$$

where C_{i0} and D_i are material parameters; $\bar{I}_1$ is the first deviatoric strain invariant defined as

$$\bar{I}_1 = \bar{\lambda}_1^2 + \bar{\lambda}_2^2 + \bar{\lambda}_3^2 \tag{A3}$$

The hyperfoam strain energy density function is given as

$$\psi = \sum_{i=1}^{N} \frac{2\mu_i}{\alpha_i^2}\left[\bar{\lambda}_1^{\alpha_i} + \bar{\lambda}_2^{\alpha_i} + \bar{\lambda}_3^{\alpha_i} - 3 + \frac{1}{\beta_i}\left(\mathrm{J}^{-\alpha_i\beta_i} - 1\right)\right] \tag{A4}$$

The best-fit parameters of the aforementioned models for the 40% H platelet-contracted clot analogous, corresponding to Figure1(G, H) is presented in Table A1.

Table A1: Material parameters of the Ogden, Yeoh, and hyperfoam models for 40% H platelet-contracted clot analogues.

Ogden model					
$\mu_1\,(kPa)$	α_1	$\mu_2\,(kPa)$	α_2	$D_1\,(1/kPa)$	$D_2\,(1/kPa)$
0.04	3.7	0.04	-3.7	0.4	0.4
Yeoh model					
C_{10}	C_{20}	C_{30}	D_1	D_2	D_3
0.012	0.025	1e-3	0.1266	0.1266	0.1266
Hyperfoam model					
$\mu_1\,(kPa)$	α_1	$\mu_2\,(kPa)$	α_2	β_1	β_2
0.04	3.25	0.04	-3.25	0.48	0.48

Appendix B: Influence of the clot viscoelasticity

Recent experimental data show that thrombus material exhibits rate-dependent visco-hyperelastic behaviour [17]. To investigate the influence of viscoelastic behaviour of thrombus material on the occlusion location, rate dependent viscoelasticity is implemented through the specification of a non- dimensional stress-relaxation curve, parameterised through a Prony series. The effective shear-relaxation modulus is given as

$$\bar{g}(t) = 1 - \sum_{i=1}^{n} g_i\left(1 - \exp(-t/\tau_i)\right) \qquad \text{(B1)}$$

where n is the number of the terms in the Prony series, τ_i are the relaxation time constants for each term of the series, while the parameters g_i sets the ratio of long-term to instantaneous effective shear modulus. A two term Prony series is implemented with $g_1 = 0.15, g_2 = 0.28, \tau_1 = 60\,\text{sec}, \tau_2 = 500\,\text{sec}$ based on a previous study from our group.

In Figure B1 two regimes of applied pressure are simulated: a single-step pressure increase, and a multi-step pressure increase. In both cases the clot eventually reaches the same final position. However, even for the case of the single-step pressure

increase the clot does not reach its final position until ~400 s after the pressure application. This suggest that taper-tube experimental measurements should be executed over several minutes following pressure application. On the other end of the spectrum, this result suggests that in vivo a clot will reach its final occluded position in the vasculature at a relatively fast time-scale of several minutes, compared to the typical elapsed time (hours) prior to clinical intervention (e.g. thrombectomy)

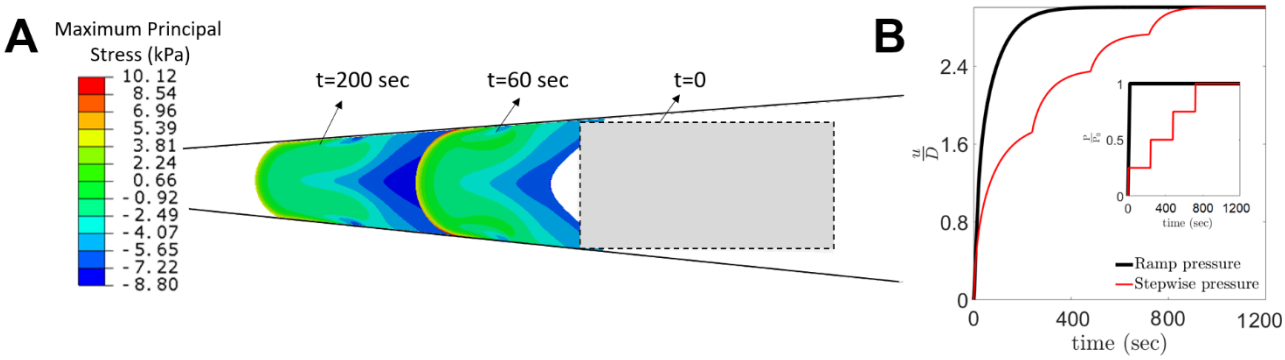

Figure B1: Influences of clot viscoelasticity on the occlusion location, u/D, in a tapered vessel. Variation of the occlusion location with time for two loading profiles (A) are shown in (B). The following parameters have been used , $P_0 = 75\ mmHg$, $L/D = 2$, $\Phi = 5^o$, $E_1 = 0.084\ kPa, E_2 = 0.25\ kPa, D_1 = 0.03, D_2 = 0.08$, $\kappa_1 = 0.15\ kPa$, $\kappa_1 = 0.75\ kPa$, $D_{1v} = 0.01, D_{2v} = 0.02, \beta_v = 0.002$, $f = 0.3$: .